Provided for non-commercial research and education use.
Not for reproduction, distribution or commercial use.

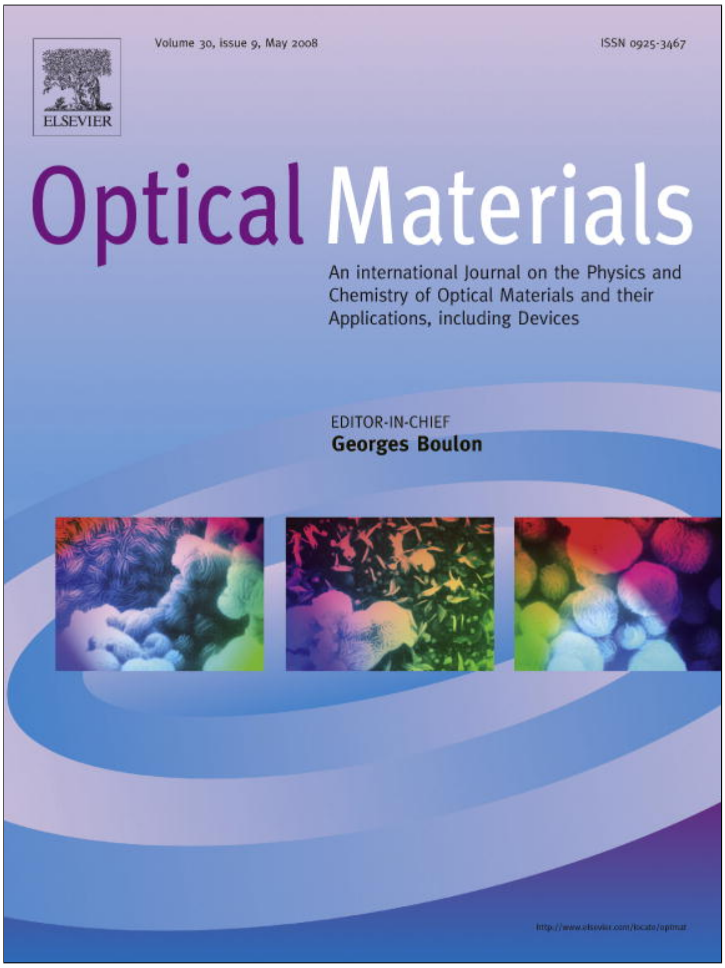

Volume 30, issue 9, May 2008

ISSN 0925-3467

ELSEVIER

Optical Materials

An international Journal on the Physics and Chemistry of Optical Materials and their Applications, including Devices

EDITOR-IN-CHIEF
Georges Boulon

http://www.elsevier.com/locate/optmat

This article appeared in a journal published by Elsevier. The attached copy is furnished to the author for internal non-commercial research and education use, including for instruction at the authors institution and sharing with colleagues.

Other uses, including reproduction and distribution, or selling or licensing copies, or posting to personal, institutional or third party websites are prohibited.

In most cases authors are permitted to post their version of the article (e.g. in Word or Tex form) to their personal website or institutional repository. Authors requiring further information regarding Elsevier's archiving and manuscript policies are encouraged to visit:

http://www.elsevier.com/copyright

Available online at www.sciencedirect.com

Optical Materials 30 (2008) 1432–1439

www.elsevier.com/locate/optmat

The entrapment of organic dyes into sol–gel matrix: Experimental results and modeling for photonic applications

Sheila C.S. Costa [a], Rodrigo M. Gester [b], Jeconias R. Guimarães [b], Jarlesson G. Amazonas [b], Jordan Del Nero [c,*], Sidicleia B.C. Silva [d], Andre Galembeck [d]

[a] *Pós-Graduação em Eng. Elétrica, UFPA, Brazil*
[b] *Pós-Graduação em Física, UFPA, Brazil*
[c] *Departamento de Física; UFPA, 66075-110, Belém, PA, Brazil*
[d] *Departamento de Química Fundamental, Universidade Federal de Pernambuco, Av. Prof. Moraes Rego, s/n CDU, CEP 50670-901 Recife, PE, Brazil*

Received 3 July 2006; received in revised form 14 August 2007; accepted 31 August 2007
Available online 24 October 2007

Abstract

To better understand the electronic absorption spectra in the UV–vis region of the methyl red (MR) dye in its anionic, isoelectronic and zwitterionic forms in aqueous solution, high level sequential-Monte Carlo/quantum mechanics (s-MC/QM) methodology was performed and compared to experimental measurements. The theoretical procedure consists in treating the solute–solvent system separately using classical MC simulations to build the MR aqueous solution and then, the MC structures are treated by quantum approaches. Thus, the solvent effects were investigated including on the INDO/CI-S calculations initially the micro and further the first hydration shells. As we excepted the absorption spectra are characterized by a strong band placed in the region of lowest energies. To the basic form we computed shoulders at 434.33 ± 0.09 and 436.34 ± 0.56 nm corresponding to the micro and first hydration shells, respectively. Our experimental measurements display this shoulder at 431 nm. Under acidic forms (isoelectronic and zwitterionic), we computed the red shift in relation to the basic compound. To the isoelectronic structure we found the absorption maximum located at 485.80 ± 0.34 and 480.66 ± 0.67 nm to the micro and first shells, respectively. The experimental prediction of 513 nm is in good agreement with theoretical result. Finally the zwitterionic form we did not obtain a micro layer, therefore we used only the first shell. Our theoretical results are converged to 502.13 ± 0.79 nm in good concordance with the experimental confirmation of 511 nm.

These samples were optically transparent, hard and resistant to dye leaching and to chemical attacks, being promising materials to be used in optical devices.

© 2007 Elsevier B.V. All rights reserved.

1. Introduction

The entrapment of dyes into solid inorganic matrices has attracted a wide interest over the last decade due to their potential applications as laser materials, photonic devices, sensors and nonlinear optical (NLO) materials [1,2].

The sol–gel process provides very attractive pathways to develop hybrid materials in which optically active species can be embedded in inorganic or organic–inorganic networks [3]. There are many recent reports in the literature dealing with sensors for ammonia [4], oxygen [5], pH [6] and temperature [7] based in sol–gel materials.

As an example of a laser device, it has recently been identified that the photostability of the dye determines the longevity of the solid-state dye laser in which it is used [8]. They found that the rate of photobleaching decreased when the glass was lasing, as compared to the case when the optical cavity was blocked modeled by a classical model. Also, the same authors found a dependence of dye with the lasing ability, i.e. the dyes lose their ability to work as a laser in acidic solution [9].

---

[*] Corresponding author. Tel.: +55 91 3201 7423; fax: +55 91 3201 7603.
E-mail address: jordan@ufpa.br (J.D. Nero).

0925-3467/$ - see front matter © 2007 Elsevier B.V. All rights reserved.
doi:10.1016/j.optmat.2007.08.008

A molecule inside a solid matrix acting as a sensor can be, also, a probe for the local structure in which it is inserted. The internal microenvironment of sol–gel derived organic–inorganic nanocomposites, for instance, can be investigated if fluorescent species are placed within [10].

Gallas et al. present a high-pressure technique coupled sol–gel method [11]. The experimental results showed that the silica–gel methodology under high-pressure produce sol–gel with low porosity and dye entrapment. The dye incorporated maintains the same optical properties as in solution, i.e equivalent dispersion in a molecular level.

Changes in the pH of the liquid phase within a gel can be followed if an acid–base indicator is dissolved in it. In a previous work, we reported the entrapment of methyl orange (MO) dye in its acidic form within aluminum polyphosphate (APP) gels. The dye was deprotonated upon exposure to gaseous ammonia, which was followed by absorption spectroscopy. In the same work, the results dealing with MO-water molecules interactions obtained by theoretical calculations were presented[12].

Recently, powerful theoretical tools have been presented to modeling materials for photonic applications. Franco et al. described a model based on classical electrodynamics for dye doped sol–gel amorphous films with a side chain and mesostructured with host–guest interactions. The results presented a very good fit to optical absorption experimental data [13]. Also, Speranza et al. explored the electronegativity equalization method (EEM) to correlate binding energy values with the electric charge distribution in praseodymium doped zinc borate glasses with a good agreement with X-ray photoelectron spectroscopy data [14].

In this paper, the sequential Monte Carlo/quantum mechanics (s-MC/QM) methodology was employed [15] to calculate the electronic absorption spectra of APP-gel included with methyl red (MR, Fig. 1) dye, which also presents NLO properties [16,17]. A cavity composed of a 1000 solvent molecules and one MR molecule as the solute was generated. This system was modeled using Monte Carlo simulation and statistically uncorrelated configurations for the quantum mechanical (QM) calculations of electronic absorption spectra. The MC simulation is carried out in the NVT ensemble and the QM calculations are performed at Hartree–Fock derivative level of theory and all average values reported here are indeed statistically converged.

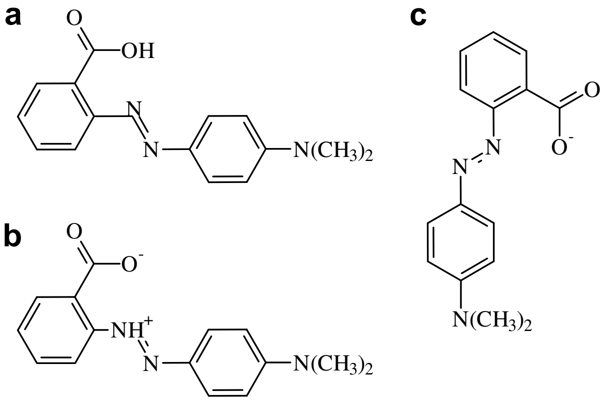

Fig. 1. Methyl red structures: (a) isoelectronic; (b) zwitterionic and; (c) anionic forms. Both geometries have the same π-electrons number and are also neutral systems. However, the main difference is the visible charge separation. The ionic form is preferred in basic conditions.

We also incorporated the methyl red dye within an aluminum polyphosphate gel which provides a viscous constricted environment to the guest molecules that avoid solute–solute associations.

2. Methodology

2.1. Aluminum polyphosphate/methyl red (APP/MR) synthesis

Aluminum nitrate, sodium polyphosphate and methyl red were used as received. The gels were prepared starting from sodium polyphosphate (2.0 mol L^{-1} in phosphorus) and 1.0 mol L^{-1} $Al(NO_3)_3$ aqueous solutions. The MR methanolic solution (6.5×10^{-5} mol L^{-1}) was previously added to the polyphosphate solution. The procedure was similar to that described earlier for the methyl orange incorporation within the APP network [12].

The solutions were mixed at room temperature under strong stirring. Gelation proceeded within 1 min, leading to a viscous mass, which was stirred and centrifuged. Under centrifugation, a supernatant solution was separated from the gel and discarded. The gel was washed with distilled water and stored in closed vials. Transparent red samples formed after 12 h resulting from gel syneresis.

Thick, self-standing APP/MR films were prepared by pressing gel samples between two polyethylene films and allowing them to dry in moisture controlled boxes at nearly 50% relative humidity, for one week. The APP/MR samples and MR solutions under different pHs (5 μL MR in 5 mL aqueous solution) were characterized by absorption spectra using a using an UV–vis spectrophotometer Perkin–Elmer LAMBDA 6 model 2688-002, within the 800–200 nm range.

2.2. Theoretical methodology

A methyl red aqueous solution is composed of one solute molecule, and a thousand water molecules were simulated by Monte Carlo (MC) computational calculations. Classic calculations were performed in the NVT ensemble at 298.15 K and at atmospheric pressure. The cubic box size L and the cutoff radius $r_c = L/2$ were modulated by the experimental water density (0.9966 g/cm^3) which it can be seen in Table 1.

The simulations were carried out stepwise: (i) in the thermalization stage only configurations that decrease the system energy were generated; (ii) in the average stage, configurations with connection energy that oscillate around the average were accepted.

Table 1
Box size and the limits for the micro and first shells (see text) for methyl red aqueous solutions; the distances are in Å. N_s refers to the number of water molecules in each shell

Methyl red	Box size	Micro shell				First shell			
		Start	Max.	End	N_s	Start	Max.	End	N_s
Basic	31.2301	1.2	1.7	2.0	6	2.0	2.8	5.3	77
Isoelectronic	31.2307	1.4	1.7	1.9	3	1.9	2.7	4.3	77
Zwitterionic	31.2307		–	–	–	2.0	2.7	4.3	73

N_s refers to the number of water molecules in each shell.
Start, max., end means the beginning, the maximum and the final part of solvation shell, respectively.

We performed 8×10^6 and 9×10^6 MC steps in the thermalization and the average stages, respectively. Here, we used as the MC step definition when all molecules of a system are systematically visited. To each molecule, all axes are randomly chosen and translated by δr, only after its axes are rotated by $\delta\theta$. Necessarily, δr is very small and the angle $\delta\theta \approx \pm 15°$. In MC simulations, the first configuration is randomly generated and using a sample procedure, like the Metropolis technique [18], configurations that reduce the bond energy are selected. Then it was possible to build a configuration chain known as Markov's chain. The molecular interactions were simulated using the Lennard-Jones plus Coulomb potentials

$$U_{ab} = \sum_i^a \sum_j^b 4\varepsilon_{ij}\left[\left(\frac{\sigma_{ij}}{r_{ij}}\right)^{12} - \left(\frac{\sigma_{ij}}{r_{ij}}\right)^{6}\right] + \frac{e^2}{4\pi\varepsilon_0}\frac{q_i q_j}{r_{ij}} \qquad (1)$$

where the sums were performed on all atomic sites of each of the molecules a and b. The $\varepsilon_{ij} = \sqrt{\varepsilon_i \varepsilon_j}$ and $\sigma_{ij} = \sqrt{\sigma_i \sigma_j}$, are geometric averages of atomic parameters εi and σi These numbers reproduce the potential energy and the distance to each atomic site in equilibrium conditions. The parameter qi was used to represent the electronic charge on each atomic site.

For the three MR forms studied, the potential parameters ε_i and σ_i are extracted of OPLS (optimized parameters for liquid simulation) developed by Jorgensen's Group [19]. Regarding to the charges, we used the HF/6-31G* calculations coupled to CHELPG procedure, both implemented by Gaussian program [20]. In the same level of calculations, we obtained all geometries of minimal energy.

Finally, to describe the water molecules, we used the SPC potential developed by van Gusteren and co-workers [21]. The molecular interactions are limited by the cutoff radius r_c, defined as half of the box size. To regions beyond this point the long range correction of potential energy is used. The long-range correction for Coulomb potential was evaluated using the reaction field methodology with dipole interactions (dielectric constant of water $\varepsilon = 78.5$) and to the Lennard-Jones potential we use the pair radial distribution function.

Nearly 800 configurations were obtained for each system. However, the structures were generated simultaneously after the previous calculations did not give new information about the systems. One way to reduce the excess of configurations is using the concept of autocorrelation function of energy $C(n)$

$$C(n) = \frac{\langle \delta E_i E_{i+n} \rangle}{\langle \delta E^2 \rangle} = \frac{\langle E_i E_{i+n} \rangle - \langle E_i \rangle \langle E_{i+n} \rangle}{\langle E^2 \rangle - \langle E \rangle^2} \qquad (2)$$

For Markovian processes, the autocorrelation function of energy is given by an exponential decay as $C(n) = \exp(-n/\tau)$. In the liquid state, specifically, $C(n)$ can be represented by a second-order exponential [22]:

$$C(n) = a_1 e^{-n/\tau_1} + a_2 e^{-n/\tau_2} \qquad (3)$$

With $C(n)$ it is possible to determine the interval in which the configurations are statistically correlated. This interval is called correlation time, τ, and can be calculated by

$$\tau = \int_0^\infty C(n)\mathrm{d}n \qquad (4)$$

The limits in the above integral are justified if one consider that, at $C(0) = 1$, two configurations are 100% correlated and at $C(\infty) = 0$ these configurations are fully uncorrelated. Thus, the correlation time to liquid systems can be written as *a1τ1 + a2τ2*. Commonly, configurations are sufficiently uncorrelated when structures separated by $n = 2\tau$ are selected. Therefore, using the energy autocorrelation function, we reduced the configuration number from 800 structures to approximately 160 configurations statistically correlated in just 21%.

It is not necessary to treat all molecules to obtain their electronic properties. Truthfully, analyzing the radial distribution function (RDF) one is be able to identify the number of molecules in the solvation layers [23]. This means that only the solvent molecules that truly interact with the solute can be considered. A systematic application of these procedures reduces the computational expenditure.

The INDO/CIS-S (intermediate neglect of differential orbital/configuration interaction spectroscopic-Single excitation) method was applied to obtain the electronic absorption spectra [24,25]. This method was specifically designed to describe the optical UV–vis transitions of organic compounds [26–31]. However, as several MC configurations are generated, it was necessary to obtain the statistical average performed on the ensemble. Also, as the appropriate Boltzmann's factor is included in the Metropolis sampling technique and the quantum properties are obtained as simple averages:

$$\langle E \rangle = \frac{1}{l} \sum_{i}^{N} E_i \tag{5}$$

a configuration chain of size l. E_i is the *eigenvalue* measured on each MC configuration. A statistical error is generated due to finite size of the configuration chain. This error can be computed as

$$\sigma = \frac{s}{\sqrt{l-1}} \tag{6}$$

where s is the standard deviation

$$s = \sqrt{\frac{l}{l-1}\left(\langle E^2 \rangle - \langle E \rangle^2\right)} \tag{7}$$

Local electronic density of states (DOS) was also calculated. The geometrical data used in this calculation were coupled by *ab initio* geometries. The results obtained indicate that the mixtures between sigma and pi electrons are quite small. Therefore, we treated the system as a π system with one orbital per site and represent the electronic Hamiltonian for the p_z for atoms through first neighbor interactions with tight binding model:

$$H = \sum_i \alpha_i |i\rangle\langle i| + \beta_{i,i+1} |i\rangle\langle i+1| + h.c. \tag{8}$$

The α index in the Hamiltonian corresponds to the negative of the ionization potential following the Clementi parametrization and β is the interaction between neighbors given by:

$$\beta_{i,i+1} = -(k/2)[I_i + I_{i+1}]S_{i,i+1} \tag{9}$$

were k is the Hückel constant equal to 1.75, $I_i = \alpha_i$, and $S_{i,i+1}$ corresponds to the overlap between the neighbors given by Slater type orbitals (Here the geometry came from *ab initio* calculations).

3. Results and discussion

3.1. Under basic pH conditions

Our experimental and theoretical measures of the UV–vis absorption spectra of the MR under basic pH nature of the UV–vis spectra are characterized by a wide band placed in the region of lowest energies and that extend from 350 to 500 nm. In this region we report a maximum absorption at 431 nm in concordance with measures previously reported in several organic and inorganic environments [32–34].

Using the theoretical approaches the liquid structures can be better studied using the radial distribution function (RDF) concept. These functions describe how the solvation shells are filled with solvent molecules. Experimentally it can be obtained by X-ray diffraction and jet-cooling techniques [35,36]. As the treatment of 1001 molecules (one MR form plus all water) would be impracticable and it is common to treat by quantum theory only solvent molecules near the solute. Hence the RDFs have a fundamental role in theoretical approach. To the system under basic pH conditions, the RDF of all first neighbors showed two well defined regions. In Fig. 2, the nearest region of the solute starting at 1.2 Å has a peak at 1.7 Å and finishes at 2.0 Å. The spherical integration in this interval reveals us six water molecules. The other range is placed between the intervals from 2.0 Å to 5.3 Å and has a maximum at 2.8 Å. The RDF to this system is shown in Fig. 2 as well as the summary of the structural information for all simulated systems is given in Table 1. When we integrated this region spherically we found 77 water molecules. Because of the great difference in the molecule number in the two shells, we will call them as micro and first shells, respectively (the same notation will be used in the isoelectronic and zwitterionic forms). Hence, we used these two shells to obtain the electronic absorption spectra of the basic MR form. We found that the results statistically converged with just 130 quantum mechanics calculations. To the micro shell of the lowest transition region, we realized a strong band centered at 434.33 ± 0.09 nm. With the calculations performed in the first shell a band centered at 436.34 ± 0.56 nm is observed. The averages to both micro and first shells are displayed in Fig. 3. Table 2 is a resume and incorporates both theoretical and experimental measures to three investigated systems. Comparing the results to basic form we concluded that the data of both shells are in good agreement with the experimental measures.

3.2. Under acidic pH conditions

Under acidic conditions the MR can be found under isoelectronic and zwitterionic forms. Both systems are elec-

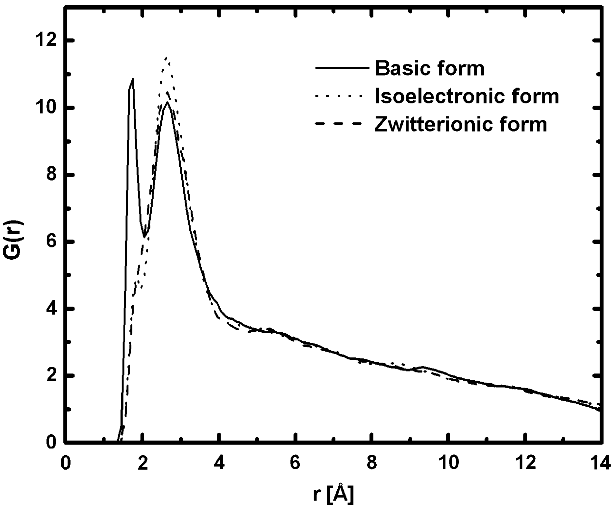

Fig. 2. Radial distribution function (RDF) for methyl red (isoelectronic, zwitterionic and anionic forms) and nearest neighbors in aqueous medium. For the basic form (line) it is easy to note the micro and first shells. For the isoelectronic form (dot), the peak corresponds to the pronounced micro shell.

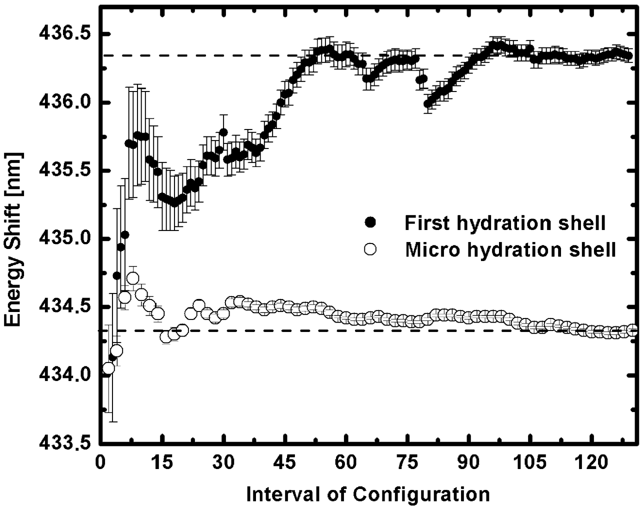

Fig. 3. Converged values for absorption maxima calculated for MR anionic form surrounded by the first and micro solvation shells (in the regions of lowest energies). The averages were obtained with about 80 quantum mechanics calculations performed on MC structures. These results are a strong evidence that this system can be described in terms of few molecules.

Table 2
Converged maximum absorption values for methyl red, calculated with the s-MC/QM methodology and obtained experimentally

Methyl red	Micro shell	First shell	Experimental
Basic	434.33 ± 0.09	436.34 ± 0.56	431
Isoelectronic	485.80 ± 0.34	480.66 ± 0.67	513
Zwitterionic	–	502.13 ± 0.79	511

All values are in nanometers (nm).

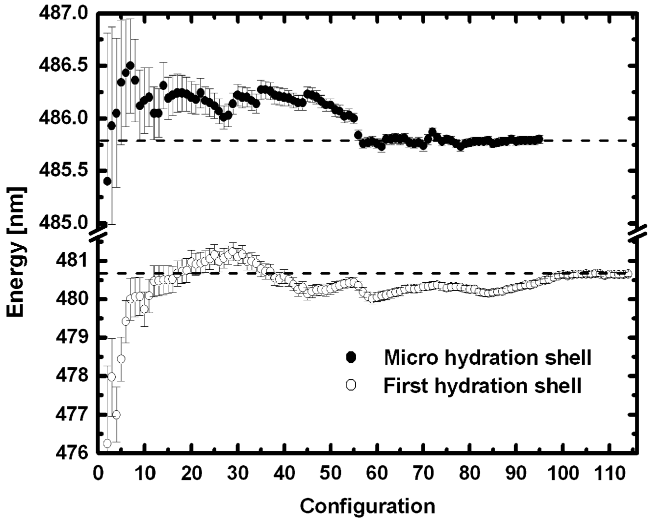

Fig. 4. Converged values for absorption maxima calculated for MR isoelectronic form surrounded by the first and micro solvation shells. Here it is possible to note that the results obtained with the micro solvation shell (3 waters) are enough to describe the electronic spectra of the system.

tronically neutral, but the second structure is characterized by a visible charge separation. These features can be easily seen in the Fig. 1.

About the electronic transitions, the isoelectronic form also presents a wide band located in the region of lowest energies. Experimentally we verified that this area extends from 450 to 600 nm with an absorption maximum located at 519.6 nm. To also describe the acidic systems, we employed the s-MC/QM procedure. The isoelectronic structures also show a micro shell placed between 1.4 and 1.9 Å and with its spherical integration we found three water molecules. Submitting the uncorrelated MC structures generated in the simulation, we obtained the spectrum of each configuration. In Fig. 4 we present the peak of absorption spectra of the micro and first hydration shell. When we considered just the micro hydration shell we found an average of 485.80 ± 0.34 nm to the lowest energies. Treating the first shell that is placed between 1.9 and 4.3 Å, we found 77 water molecules. To the lowest energies our quantum calculations showed a maximum of absorption centered at 480.66 ± 0.67 nm.

To compute the maximum absorption in the region of the lowest transitions, we used about 153 quantum mechanics calculations on MC configurations composed by one zwitterionic MR form plus the 73 water molecules found in the first solvation shell. We obtained a converged value at 502.13 ± 0.79 nm. The convergence to this excitation is depicted in Fig. 5. The experimental measurements have shown a wide band between 450 and 600 nm with a shoulder at 518.5 nm.

Also, there is a large possibility that all water molecules placed at the micro shell can make hydrogen bond (H-bond). Remember that all RDFs shown that the micro layers start before 1.9 Å. However, some authors consider 1.9 Å as the intermediate distance to the formation of H-bonds [37]. However, associated to geometric parameters,

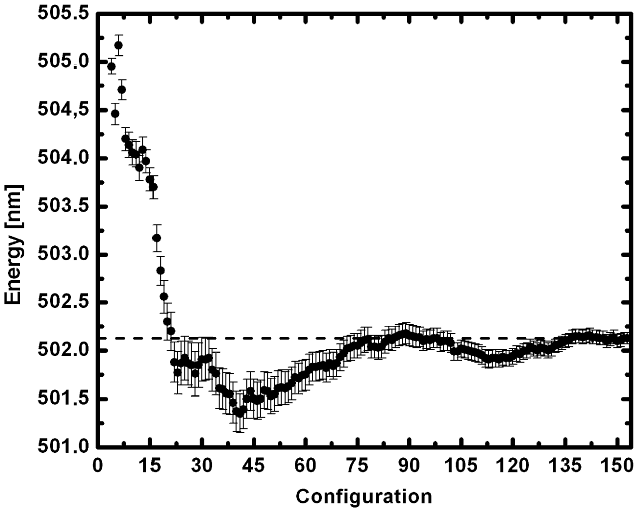

Fig. 5. Converged values for absorption maxima calculated for MR zwitterionic form surrounded by the first and micro solvation shells. 153 quantum mechanics calculations in uncorrelated configurations were generated by Monte Carlo simulations. As is visible the average is researched with about 90 configurations.

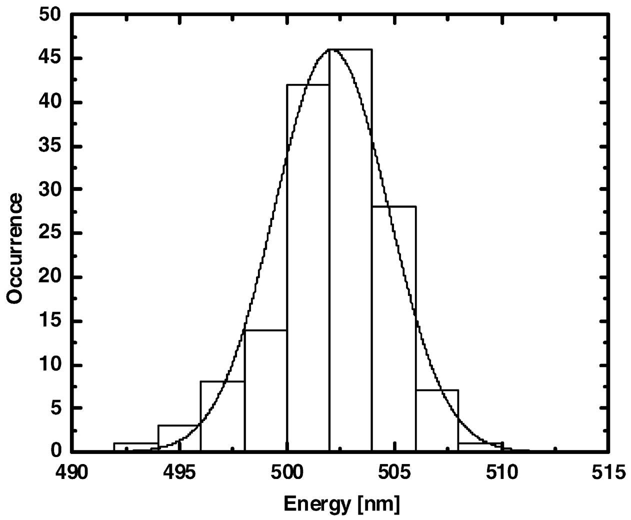

Fig. 6. A Histogram of the measurements performed in the zwitterionic structure of the methyl red generated by Monte Carlo simulations. To build this graphic we used all transition values obtained to the maximum of absorption to the lowest energies region.

as distances and angles, other works have used energetic conditions to define an H-bond with success [38]. As an example, we can analyze the isoelectronic form. Fig. 7 is a MC configuration obtained to the first hydration shell composed of three water molecules. Here all solvent molecules are located around 1.9 Å and surround the group that is O═CR─OH that is close to the main acceptor (═O) and donor (─OH) solvent group. Fig. 8 is the superposition of all MC configurations generated to this shell. We can clearly see that the above situation is not isolated because there exists an accumulation around the O═CR─OH solute group. In this study we do not compute the real H-bond contributions in the electronic transitions. However, based only in geometrical considerations we believe that H-bond interactions can be represented by information obtained with the micro shells calculations.

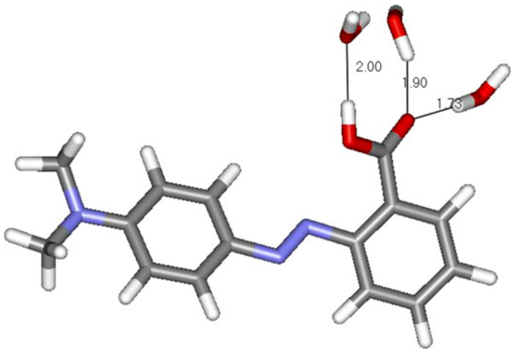

Fig. 7. A Monte Carlo generated configuration for methyl red isoelectronic form and three nearest water molecules, situated in the vicinity of the carboxylate group. Solvent molecules are at 1.7–2.0 Å from the solute molecule.

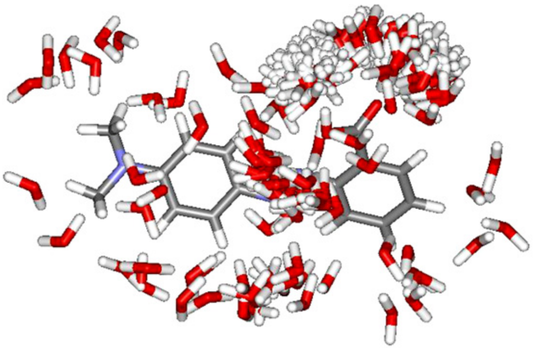

Fig. 8. Superposition of all Monte Carlo structures generated by MR isoelectronic form surrounded by nearest and nest-nearest neighbors. Note the accumulation of water molecules around carboxylate N═N groups which are capable to form hydrogen bonds

3.3. Statistical convergence

All theoretical measurements done until this moment are performed on systems generated by stochastic procedures. Hence there is the needful of to investigate the statistical convergence of theoretical results presented before. As an example we will discuss more directly on only zwitterionic structure. However, all conclusions must be extended to others systems. We expected that only a reduced number of MC configurations are necessary to research the average. However, the single restriction is that these structures be statistically uncorrelated. One way to determine which configurations could be chosen is using the autocorrelation function of energy $C(n)$. This feature can be easily verified in Fig. 5. It is visible that the convergence is found with about 90 quantum calculations performed on MC configurations. If we analyze the Eqs. (5) and (6), we can conclude that when the size chain l is increased the statistical error and the standard deviation tend to zero and to constant values, respectively. Once again these observations are evident in Fig. 5. Fig. 6 is the histogram built to the zwitterionic system. Additionally, the other important observation is that about 57% of the transitions are located between $\langle E \rangle \pm s$ which correspond to the interval from 501.34 to 502.92 nm.

3.4. Experimental spectra

In Fig. 9 it is presented the system when the dye was incorporated within the polyphosphate gel under different pHs: (I) The spectrum of the basic form showing a typical transition ascribed to MR with a maximum located near 431 nm. Upon exposure to ammonia vapor, some samples turned yellow. When the exposure is stopped they acquire a pale yellow coloration. (II) and (III) present spectra of the acidic forms showing typical transitions ascribed to MR with a maximum located near 513 nm and 511 nm. Fresh MR/APP spectrum resembles the MR spectrum acquired from an aqueous solution at pH 3.3. Hence, it seems that the chemical environment around the dye guest molecule is very similar to that observed in the liquid.

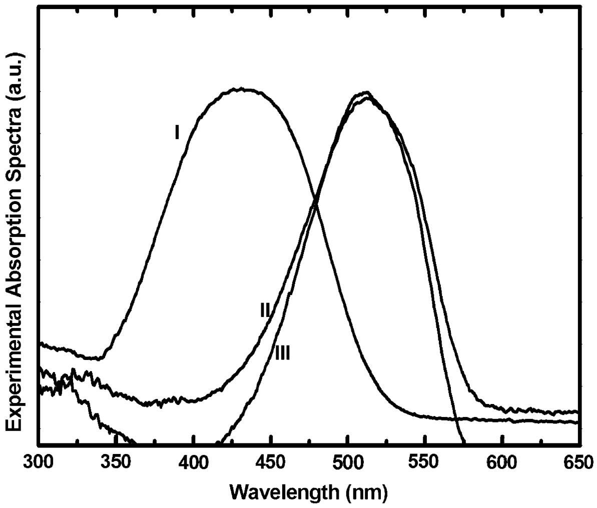

Fig. 9. Experimental absorption spectra for (I) isoelectronic; (II) zwitterionic and (III) anionic forms.

3.5. Electronic density of states

For completeness, in Fig. 10 presents the local density of states of MR in acidic and basic forms showing the presence of 17 [18] states of basic [acidic] form and band structure of $\sim$230 meV for all bands. A two-level HOMO (charged system) is presented centered in –13.18 eV for basic form. Although a two-level HOMO is presented slightly blue-shifted, centered in –13.05 eV for acidic form. The LUMO level for basic [acidic] is a single level centered in -12.30 eV [-12.55 eV] presenting a LUMO-HOMO equal to 0.88 eV [0.50 eV]. This energy range is a typical gap of an organic semiconductor, widely used to fabricate diodes [39] and transistors [40]. As organic semiconductor-*type*, these results are in good agreement with the recent experimental one suggesting that MR could be used as a Schottky barrier diode [41].

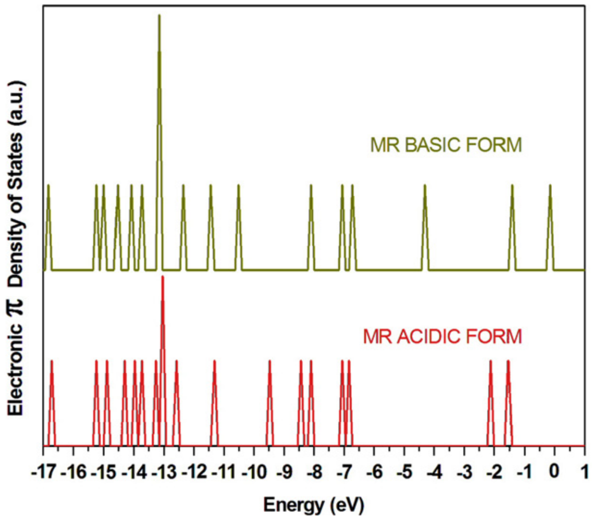

Fig. 10. Local electronic π density of states (DOS) for methyl red on anionic and isoelectronic forms.

4. Summary and conclusions

In the present paper, we analyze the solvent effects in the electronic UV absorption spectra of MR in its basic and acidic (isoelectronic and zwitterionic) forms through the Sequential-Monte Carlo/quantum mechanical approach. The autocorrelation function of the energy was applied in this implementation in order to reduce the number of QM calculations during all calculation.

In summary for basic, acidic and zwitterionic forms we found out experimental shoulders as 431 nm, 513 nm and 511 nm, respectively. Our theoretical results corresponding to basic, acidic and zwitterionic forms are 436.34 ± 0.56 nm, 480.66 ± 0.67 nm and 502.13 ± 0.79 nm for the first solvation shell.

Overall these results are in very good accordance within the experimental/theoretical results. These theoretical results correspond an error less than 4.0% to the experimental one. This work is part of a more complete investigation on pH organic indicators systems to be reported elsewhere.

Acknowledgments

SCSC thanks a D.Sc. CAPES fellowship. RMG, JGA and JRG thank M.Sc. CAPES fellowship. JDN's group is *deeply grateful* to Prof. Sylvio Canuto for providing the computer program DICE [42] for Monte Carlo simulation.

References

[1] P.N. Prasad, D.J. Williams, Introduction to Nonlinear Optics Effects in Molecules and Polymers, Wiley, New York, 1991.
[2] F. Chaumel, H. Jiang, A. Kakkar, Chem. Mater. 13 (2001) 3389.
[3] C. Sanchez, B. Lebeau, F. Chaput, J.P. Boilot, Adv. Mater. 15 (2003) 1969.
[4] S.Q. Tao, L. Xu, J.C. Fanguy, Sensor. Actuat. B 115 (2006) 158.
[5] B. Konig, O. Kohls, G. Holst, R.N. Glud, M. Kuhl, Marine Chem. 97 (2005) 262.
[6] C.Y. Li, X.B. Zhang, Z.X. Han, B. Akermark, L.C. Sun, G.L. Shen, R.Q. Yu, Analyst 131 (2006) 388.
[7] M.C. Burt, B.C. Dave, Sensor. Actuat. B 107 (2005) 552.
[8] A.M. Weiss, E. Yariv, R. Reisfeld, Opt. Mat. 24 (2003) 31.
[9] E. Yariv, R. Reisfeld, Opt. Mat. 13 (1999) 49.
[10] T. Keeling-Tucker, J.D. Brennan, Chem. Mater. 13 (2001) 3331.
[11] T.M.H. Costa, H.S. Hoffmann, E.V. Benvenutti, V. Stefani, M.R. Gallas, Opt. Mat. 27 (2005) 1819.
[12] A. Galembeck, S.B.C. Silva, J.A.P. Silva, J. Del Nero, Opt. Mat. 24 (2004) 637.
[13] A. Franco, G. Valverde-Aguilar, J. Garcia-Macedo, Opt. Mat. 29 (2006) 6.
[14] G. Speranza, L. Minati, M. Anderle, Opt. Mat. 28 (2006) 1258.
[15] V. Ludwig, P.K. Mukherjee, K. Coutinho, S. Canuto, Phys. Rev. A 72 (2005) 062714.
[16] C. Khoo, M.Y. Shih, A. Shishido, P.H. Chen, M.V. Wood, Opt. Mat. 18 (2001) 85.
[17] L. Frey, M. Kaczmarek, J.-M. Jonathan, G. Roosen, Opt. Mat. 18 (2001) 91.
[18] N. Metropolis, A.W. Rosenbluth, M.N. Rosenbluth, A.H. Teller, E. Teller, J. Chem. Phys. 21 (1953) 1087.

[19] W.L. Jorgensen, D.S. Maxwell, J. Tirado-Rives, J. Am. Chem. Soc. 118 (1996) 11225.

[20] M.J Frisch, G.W Trucks, H.B Schlegel, et al., Gaussian, Inc., Pittsburgh PA, 1998.

[21] H.J.C. Berendsen, J.P.M. Postma, W.F. van Gusteren, J. Hermans, in: B. Pullman (Ed.), Intermolecular Forces, Reidel, Dordrecht, 1981, p. 331.

[22] K. Coutinho, S. Canuto, J. Mol. Struct. (Theochem) 632 (2003) 235.

[23] Y. Choi, K.W. Cho, K. Jeong, S. Jung, Carbohyd. Res. 341 (2006) 1020.

[24] J. Ridley, M.C. Zerner, Theor. Chim. Acta 32 (1973) 111.

[25] J.D. Head, M.C. Zerner, Chem. Phys. Lett. 131 (1986) 359.

[26] J. Del Nero, B. Laks, Synth. Met. 101 (1999) 440.

[27] J. Del Nero, B. Laks, Synth. Met. 101 (1999) 379.

[28] J. Del Nero, C.P. de Melo, Opt. Mat. 21 (2003) 455.

[29] J. Del Nero, C.P. de Melo, Synth. Met. 121 (2001) 1741.

[30] J. Del Nero, B. Laks, Synth. Met. 84 (1997) 423.

[31] J. Del Nero, R.E. de Araujo, A.S.L. Gomes, C.P. de Melo, J. Chem. Phys. 122 (2005) 104506.

[32] M.S. Masoud, H.H. Hammud, Spectroch. Acta Part A 57 (2001) 977.

[33] G. Seu, Dyes and Pigm. 29 (1995) 227.

[34] S.S. Ashraf, M.A. Rauf, S. Alhadrami, Dyes and Pigm. 69 (2006) 74.

[35] H. Saitoh, K. Ohshima, K. Tsubouchi, Y. Takasu, H. Yamada, I. J. Biol. Macromol. 34 (2004) 259.

[36] A.A. Shama, H.M. Zeyada, Opt. Mat. 24 (2003) 555.

[37] M.A.M. Cordeiro, W.P. Santana, R. Cusinato, J.M.M. Cordeiro, J. Mol. Struct. (Theochem) 759 (2006) 159.

[38] T. Malaspina, K. Coutinho, S. Canuto, J. Chem. Phys. 117 (2002) 1692.

[39] A. Saraiva-Souza, C.P. de Melo, P. Peixoto, J. Del Nero, Opt. Mat. 29 (2007) 1010.

[40] A. Saraiva-Souza, R.M. Gester, M.A.L. Reis, F.M. Souza, J. Del Nero, J. Comp. Theor. Nanoscience, in press.

[41] T. Kilicoglu, M.E. Aydin, Y.S. Ocak, Physica B 388 (2007) 244.

[42] K. Coutinho, S. Canuto, DICE: A Monte Carlo program for molecular liquid simulation, University of São Paulo, Brazil, version 2.9, 2003.